Realtime measurement of phase partitioning of organic compounds using a Proton-Transfer-Reaction Time-of-Flight Mass Spectrometer coupled to a CHARON inlet

Yarong Peng[1,2], Hongli Wang[2,*], Yaqin Gao[2], Shengao Jing[2], Shuhui Zhu[2], Dandan Huang[2], Peizhi Hao[3], Shengrong Lou[2], Tiantao Cheng[4,5,*], Cheng Huang[2], Xuan Zhang[3,*]

[1] Department of Environmental Science and Engineering, Fudan University, Shanghai, 200438, China

[2] State Environmental Protection Key Laboratory of Formation and Prevention of Urban Air Pollution Complex, Shanghai Academy of Environmental Sciences, Shanghai, 200233, China

[3] School of Natural Sciences, University of California, Merced, 95343, USA

[4] Department of Atmospheric and Oceanic Sciences, Fudan University, Shanghai, 200438, China

[5] Big Data Institute for Carbon Emission and Environmental Pollution, Fudan University, Shanghai, 200438, China

Correspondence to: Hongli Wang (wanghl@saes.sh.cn), Tiantao Cheng (ttcheng@fudan.edu.cn), Xuan Zhang (xzhang87@ucmerced.edu)

18   **Abstract.** Understanding the gas-particle partitioning of semivolatile organic compounds

19   (SVOCs) is of crucial importance in the accurate representation of the global budget of

20   atmospheric organic aerosols. In this study, we quantified the gas- vs. particle-phase fractions

21   of a large number of SVOCs in real time in an urban area of East China with the use of a

22   CHemical Analysis of aeRosols ONline (CHARON) inlet coupled to a high resolution Proton

23   Transfer Reaction Time-of-Flight Mass Spectrometer (PTR-ToF-MS). We demonstrated the

24   use of the CHARON inlet for highly efficient collection of particulate SVOCs while

25   maintaining the intact molecular structures of these compounds. The collected month-long

26   dataset with hourly resolution allows us to examine the gas-particle partitioning of a variety of

27   SVOCs under ambient conditions. By comparing the measurements with model predictions

28   using the instantaneous equilibrium partitioning theory, we found that the dissociation of large

29   parent molecules during the PTR ionization process likely introduces large uncertainties to the

30   measured gas- vs. particle-phase fractions of less oxidized SVOCs, and therefore, caution

31   should be taken when linking the molecular composition to the particle volatility when

32   interpreting the PTR-ToF-MS data. Our analysis suggests that understanding the fragmentation

33   mechanism of SVOCs and accounting for the neutral losses of small moieties during the

34   molecular feature extraction from the raw PTR mass spectra could reduce, to a large extent, the

35   uncertainties associated with the gas-particle partitioning measurement of SVOCs in the

36   ambient atmosphere.

37

38   **1. Introduction**

39   Gas-particle partitioning of semivolatile organic compounds (SVOCs) is a critical process

40   involved in the formation and evolution of atmospheric organic aerosols (OA). Traditionally,

gas-particle equilibrium partitioning of organic substances is assumed to be established instantaneously (Zhang and Seinfeld, 2013), this assumption is in question if particles are semi-solid or glassy (Shiraiwa et al., 2013). Most studies to date addressing the kinetic limitations in partitioning have used indirect and/or theoretical methods that are lack of chemical and molecular specificity (Mai et al., 2015; Shiraiwa and Seinfeld, 2012). Direct measurements of gas-particle partitioning of SVOCs are needed in order to develop accurate parameterizations for the organic aerosol formation in climate models.

The major challenge in the characterization of gas-particle partitioning of SVOCs lies in the realtime measurement of labile compounds while maintaining their intact molecular structures with minimal fragmentation (Zhang et al., 2016a; Zhang et al., 2016b; Zhang et al., 2019). In recent years, soft ionization techniques coupled to mass spectrometry have been widely used for the measurement of gas-phase SVOCs at the molecular level (Veres et al., 2008; Crounse et al., 2006; Heald and Kroll, 2020). Combined with thermal desorption methods, these techniques have also been deployed to measure organic compounds in both gas and particle phases nearly simultaneously (Krechmer et al., 2016). A notable example would be the use of the Filter Inlet for Gases and AEROsols coupled with the Chemical Ionization Mass Spectrometry (FIGAERO-CIMS) to quantify the gas-particle partitioning of a broad range of organic compounds in real time (Lopez-Hilfiker et al., 2014; Ye et al., 2021; Voliotis et al., 2021; Wang et al., 2020a; Lutz et al., 2019; Lee et al., 2018; Le Breton et al., 2018; Stark et al., 2017; Lopez-Hilfiker et al., 2016; Lopez-Hilfiker et al., 2015; Palm et al., 2020). A number of studies among those have reached a consensus that the thermograms method, i.e., using the calibrated thermal desorption profiles vs. temperature to derive the volatility, likely provides the best estimates of the actual phase distribution. In contrast, using the directly measured gas- and

64 particle-phase fractions of a given analyte will most likely introduce a significant positive or

65 negative bias to the volatility estimation due to the thermal decomposition of labile organic

66 compounds during the desorption process (Lopez-Hilfiker et al., 2015; Stark et al., 2017). Such

67 thermal decomposition (or ion fragmentation) artifacts, either positive or negative depending

68 on the molecular size, have been suggested to constitute the largest uncertainties in the

69 estimation of phase partitioning behaviors of SVOCs using the thermal desorption method at

70 ambient pressure (Thompson et al., 2016).

71 Along with the line of thermal desorption method development, an inlet designed for the

72 CHemical Analysis of aeRosols ONline (CHARON) has been developed and coupled to the

73 Proton Transfer Reaction Time-of-Flight Mass Spectrometer (PTR-ToF-MS) in recent years.

74 As CHARON-PTR-ToF-MS does not rely on any form of pre-concentration on surfaces, it

75 could provide online and direct measurements of organic compounds in both phases, compared

76 with traditional thermal desorption instruments which still need to address artifacts during the

77 particle collection and desorption processes. Another potential advantage of CHARON-PTR-

78 ToF-MS is that the chemical information of the collected particles can be studied qualitatively

79 and quantitatively over a chemical composition level even at sub-nanogram mass

80 concentrations per molecule owing to the well studied ion-molecule reaction chemistry in PTR-

81 ToF-MS (Piel et al., 2019). CHARON has shown promising potential in the realtime analysis

82 of the chemical composition and spatiotemporal distributions of aerosols with laboratory-,

83 ground-, and aircraft-based platforms (Piel et al., 2019; Tan et al., 2018; Gkatzelis et al., 2018a;

84 Gkatzelis et al., 2018b; Muller et al., 2017; Eichler et al., 2017; Eichler et al., 2015; Antonsen

85 et al., 2017; Leglise et al., 2019; Piel et al., 2021). As a relatively new technique, the use of

86 CHARON-PTR-ToF-MS to investigate the gas-particle partitioning of organic compounds is

87   still quite limited. Only one study by Gkatzelis et al. (2018b) deployed CHARON, together

88   with two other aerosol sampling inlets, to measure the OA formation and aging from

89   monoterpenes and real plant emissions in chamber experiments. Whether the CHARON inlet

90   can be applied to the study of gas-particle partitioning of organic compounds under the actual

91   atmospheric conditions remains to be validated.

92   In this study, we assess the applicability of the CHARON inlet to the time-resolved

93   collection of organic compounds in their native molecular state using laboratory tests with a

94   series of authentic standards. We further employ the CHARON inlet coupled to a high

95   resolution PTR-ToF-MS instrument to measure an array of gaseous and particulate SVOCs in

96   an urban area of East China. The obtained month-long hourly dataset allows us to examine the

97   gas-particle partitioning of SVOCs spanning a range of volatilities. By comparing the

98   measurements with model predictions using the instantaneous equilibrium partitioning theory,

99   we found that fragmentation during the PTR ionization process may introduce large

100 uncertainties to the measured gas- vs. particle-phase fractions of less oxidized SVOCs.

101 Understanding the dissociation patterns of parent molecules and accounting for the

102 fragmentation losses when extracting the molecular features from the raw PTR mass spectra

103 are needed to improve the measured accuracy of SVOCs partitioning between the gas and

104 particle phase.

105

106 **2.   Material and Methods**

107 **2.1. Sampling site**

108   The sampling site located in the campus of the Shanghai Academy of Environmental

109 Science (SAES) is representative of a typical urban setting surrounded by restaurants, shopping

110   malls, and residential and commercial buildings (Fig. S1). Two traffic-heavy streets in the area

111   (Caobao Road and Humin Highway) are located ~ 150 m and 450 m lateral distances to the east

112   of the sampling site. A few number of petrochemical and chemical industrial facilities are

113   located ~ 50 km to the south and southwest of the observation site, which likely bring certain

114   long-lived pollutants to the site at a typical wind speed of ~ 1 – 3 m/s. Major pollution sources

115   in the area include traffic, commercial and residential activities, and regional transport (Huang

116   et al., 2021; Peng et al., 2023). The sampling inlet of the PTR-ToF-MS instrument was installed

117   on the roof of an eight-story building ~ 24 m above the ground. A comprehensive measurement

118   of gas- and particle-phase compounds in the ambient air was performed from Oct 24 to Nov 22.

119   During the sampling period, the average temperature, relative humidity, and wind speed were

120   18.0 ± 3.0 °C, $61.0 \pm 15.0\%$, and 1.8 ± 0.7 m/s, respectively. The prevailing wind direction in

121   this region was from the northwest and north during the polluted period (Fig. S2).

122   **2.2. CHARON-PTR-ToF-MS**

123   **2.2.1.   Operation protocols**

124   A Proton Transfer Reaction Time-of-Flight Mass Spectrometer (PTR-ToF-MS) coupled to

125   a CHemical Analysis of aeRosols ONline (CHARON, Ionicon Analytik Inc, Innsbrunck,

126   Austria) inlet was employed to measure the gas- and particle-phase concentrations of a series

127   of SVOCs. The PTR-ToF-MS instrument used here is equipped with a radio frequency (RF)-

128   only quadrupole ion guide that transmits ions more efficiently (PTR-QiTOF, Ionicon Analytik

129   Inc) but results in a low-mass cutoff (Fig. S4). The operating parameters of the PTR-ToF-MS

130   were held constant during the entire measurement period. The drift tube pressure, temperature,

131   and voltage were 2.9 mbar, 120 °C, and 500 V, respectively. These conditions correspond to an

132   E/N (E is the electric field, and N is the number density of the gas molecules in the drift tube)

6

value of ~ 100 Td (1 Td = 10^{-17} V cm^2) and a reaction time of 120 µs. Note that the *E/N* value determines the collision energy of ions in the reactor and therefore the degree of fragmentation and cluster formation. The operating conditions were selected for the purpose of relatively low fragmentation intensities (compared to 120 – 140 Td) and limited production of water clusters (compared to 60 – 80 Td). Low *E/N* enhances the degree of water clustering, which complicates the analysis of analyte ions due to a complex interplay between cluster formation (RH$^+$(H$_2$O)$_n$) and proton transfer reactions (Holzinger et al., 2019). During the campaign, the sensitivity of the PTR-ToF-MS was in the range of 300 – 1000 ncps ppb^{-1} and the mass resolution was maintained at ~ 5000 m/Δm. Mass spectra were collected at a time resolution of 10 s.

The CHARON inlet consists of 1) a gas-phase denuder (GPD) for stripping off gas-phase analytes, 2) an aerodynamic lens (ADL) for particle collimation which is combined with an inertial sampler for emanating the particle-enriched flow, and 3) a thermo-desorption unit (TDU) for particle volatilization. The CHARON inlet functionality has been described in great detail by Eichler et al. (2015). The inlet we used here had a particle enrichment factor of ~ 15, as discussed shortly. The vaporizer (TDU) was operated at 140 °C and ~ 8 mbar absolute pressure. This temperature was chosen to ensure all the unknowns observed in the field can be evaporated effectively while maintaining relatively intact molecular structures, see more details in Section 3.1. Measurements of organic compounds in the gas and particle phase were conducted using a parallel sampling system with two independent pumps, allowing for the selection of flow rates specifically adjusted for each phase, resulting in the overall residence time of less than 2 s (Fig. S3).

2.2.2.   Sampling alternation between gas and particle phase

Gas-phase compounds were measured by directly sampling the ambient air via a 2 m long

156　perfluoro-alkoxy (PFA) tube (1/4'' OD) capped with a polytetrafluoroethylene (PTFE) filter

157　(Mitex^{TM} PTFE membrane, 5 μm pore size, 47 mm diameter) to prevent the clogging of

158　particles in the PTR capillaries. The gas-phase inlet was independently connected to the PTR-

159　ToF-MS instrument upstream of the drift tube via a pressure-controlled subsampling PEEK

160　capillary (1/16'' OD). Zero measurements were performed by overflowing catalytically

161　(platinum at 370°C) purified air through the inlet. Ambient particles were sampled through a

162　stainless steel tube (3/8'' OD) with a flow rate of ~ 3 L min^{-1}, out of which a flow of ~ 500 ml

163　min^{-1} was directed to the CHARON inlet. A PM$_{2.5}$ cyclone was installed in front of the sampling

164　line to remove coarse particles (> 2.5 μm). The particle-phase background was measured by

165　placing a High-Efficiency Particulate Air filter (HEPA, HEPA-CAP 7, GE Healthcare UK

166　Limited, Buckinghamshire, UK) upstream of the CHARON inlet. Servo motor activated valves

167　made of passivated stainless steel were used for switching between the two inlet configurations.

168　During the campaign, CHARON-PTR-ToF-MS automatically switched between gas and

169　particle phase every 15 min. Detailed setup is given in Fig. S3 in the Supporting Information.

170　　The built-in PTR-manager software (Ionicon Analytik GmbH, Innsbruck, Austria) offers

171　the possibility to program sequences by which the instrument switches between different

172　settings. It takes ~ 1 min for gases and particles to re-equilibrate when switching between these

173　two modes. Data generated during this transition period (~ 2 min) were not considered.

174　Instrument background was measured for 15 min every 5h. The limits of detection (LoD) at 1

175　min resolution were in the range of 5.6 ± 2.9 ng m^{-3} for gases and 0.7 ± 0.5 ng m^{-3} for particles,

176　respectively (Fig. S5). Concentrations of gaseous and particulate compounds shown here

177　included the last 5 min of every gas/particle-phase working mode, in order to minimize the

178　interferences carried over from the previous working mode by allowing for a sufficient amount

179   of equilibration time in the inlet (Piel et al., 2021). In order to synchronize the gas- and particle-

180   phase data to calculate gas-particle partitioning, the average hourly data were then used for

181   further analysis.

182   **2.2.3.   Sensitivity and calibration**

183   Weekly calibrations were performed using a multicomponent calibration gas standard

184   (Linde, USA) at five concentration levels from 0.5 to 10 ppb (Fig. S4a). The calibration mixture

185   includes methanol, acetonitrile, acetaldehyde, acrolein, acetone, isoprene, methyl vinyl ketone,

186   methyl ethyl ketone, 2-pentanone, toluene, styrene, p-xylene, 1,3,5-trimethylbenzene,

187   naphthalene and α-pinene. Calibration standards with higher molecular weight were excluded

188   because we only considered ion masses below 200 amu from the field measurement for the

189   study of gas-particle partitioning, see discussions given in Text S1. Here the sensitivity of PTR-

190   ToF-MS is defined as the normalized ion intensity of RH^+ (ncps) obtained at a mixing ratio of

191   1 ppb. For a given species (R), its sensitivity (S, ncps ppb^{-1}) is a linear function of the rate

192   constant of its reaction with H_3O^+ (k) :

$$S = \frac{\frac{I_{RH^+}}{I_{H_3O^+}} \times 10^6}{\frac{[R]}{N} \times 10^9} = k \times N \times 10^{-3} \times t \times \frac{T_{RH^+}}{T_{H_3O^+}} \times F_{RH^+} \tag{1}$$

$$\text{corrected } S = \frac{S}{\frac{T_{RH^+}}{T_{H_3O^+}} \times F_{RH^+}} = a \times k \tag{2}$$

195   where the signals of H_3O^+ ($I_{H_3O^+}$) and RH^+ ions (I_{RH^+}) measured by the mass analyzer (in cps)

196   can be related to the signals of H_3O^+ ($[H_3O^+]$) and RH^+ ($[RH^+]$) ions at the end of the drift tube,

197   using their respective transmission efficiencies ($T_{H_3O^+}$ and T_{RH^+}) from the drift tube to the

198   detector (De Gouw and Warneke, 2007). $[R]$ is the concentration of species R and N is the

199   number density of gas in the drift tube. The reaction time (t) is determined by the ion drift

velocity. F_{RH^+} represents the fraction of product ions detected as RH^+ ions ($0 \leq F_{RH^+} \leq 1$). For non-fragmenting compounds, $F_{RH^+} = 1$. The measured sensitivity is further corrected by accounting for fragmentation and transmission efficiency, the value of which was derived from laboratory experiments (Fig. S4a). Uncertainties associated with the addition of the low-mass filter have been accounted for in the regression of individual transmission efficiency measurements on corresponding mass to charge ratios. The overall relative standard deviations were less than 15%. *a* is the slope of the linear regression of the corrected sensitivities on the proton-transfer-reaction rate coefficients (k), as shown in Fig. S4b. Following the method by Sekimoto et al. (2017), the linear regression result was used to determine the sensitivities of all uncalibrated species. The overall uncertainty was less than 15% for compounds with standards and around 50% for those without standards. Calculated sensitivity based on this method agrees well with measurements of authentic standards (Fig. S4c).

2.2.4.   Enrichment factor

The CHARON inlet was calibrated routinely with pure ammonium nitrate particles to derive the enrichment factor as a function of the particle size following the procedures described in Eichler et al. (2015). In addition, we used a selection of authentic standards (Table S1) to test the effect of desorption temperature on the enrichment factor of labile compounds. Previous studies with CHARON generally used a temperature of 140 °C to vaporize particles (Leglise et al., 2019; Gkatzelis et al., 2018b; Tan et al., 2018). Herein, we tested the TDU temperature ranging from 70 to 140°C. The selected chemical standards were individually dissolved in distilled water (ethanol in the case of 2-Pentadecanone and 1-Pentadecanol) and nebulized by an atomizer (TSI 3076, Shore-view, MN, USA) that was pressurized with ultrapure zero air. The nebulizer outflow was diverted through two diffusion dryers to remove water vapor and an

activated charcoal denuder (NovaCarb F, Mast Carbon International Ltd., Guilford, UK) to
remove organic vapors. The resulting flow of polydisperse particles was then delivered into a
differential mobility analyzer (DMA, TSI 3080) for particle size selection. The transmitted
particles at a given size bin (300 nm for organics and $100 - 450$ nm range for ammonium nitrate)
were introduced into the CHARON-PTR-ToF-MS analyzer and a condensation particle counter
(CPC, TSI 3775), respectively. Particle mass concentrations were calculated based on the CPC
number distribution measurements by assuming a shape factor of 0.8 for ammonium nitrate
particles and 1 for organic particles, respectively.

The particle enrichment factor (EF) of a given analyte i was calculated as the ratio of the
PTR-ToF-MS derived vs. CPC derived mass concentrations of analyte i at a given particle size
bin:

$$VMR_{(PTR)i} = \frac{I_i}{S_i} \tag{3}$$

$$VMR_{(CPC)i} = \rho_i \times V \times N_i \times V_m / Mw_i \tag{4}$$

$$EF = \frac{VMR_{(PTR)i}}{VMR_{(CPC)i}} \tag{5}$$

where I_i is the normalized signal of species i (ncps) by PTR-ToF-MS, S_i is the sensitivity
(ncps ppb^{-1}), VMR is the volume mixing ratio (ppb), ρ is the density of species i (g cm^{-3}),
V is the volume of a particle sphere (m^3), N_i is the number concentration of particles measured
by CPC (cm^{-3}), V_m is the molar volume of an ideal gas at 1 atm (22.4 L mol^{-1}), Mw_i is the
molecular weight (g mol^{-1}). As the calculated sensitivities of most organics in the absence of
authentic standards are subject to uncertainties (15% – 50%), we will herein use the
multiplication of EF and S_i to evaluate the combined effect of CHARON enrichment and
sensitivity on the measured concentrations of a given analyte i in the particle phase.

2.2.5. Data processing

Data were analyzed using the Tofware package (v3.2.0, Tofwerk Inc), within the Igor Pro software (v7.0, Wavemetrics). Using this package, time-dependent mass calibrations were performed using four ions ($H_3^{18}O^+$, NO^+, $C_6H_5I^+$ and $C_6H_5I_2^+$), where $C_6H_5I^+$ and $C_6H_5I_2^+$ were produced from the internal standard di-iodobenzene. The relative mass deviation was within 6 − 8 ppm across the mass spectra. Considering the humidity dependence of reagent ions (H_3O^+ and $H_3O^+(H_2O)$), the fitted product ion signals (RH^+) were normalized to a standard reagent ion of 10^6 cps (counts per second). Elemental composition was determined based on the accurate *m/z* (mass to charge ratio) and isotopic pattern analysis. A list of ~ 1600 ions was extracted, including both gas- and particle-phase ions. Molecular formulas including only C, H, and O atoms were assigned to the detected ions by the addition of one proton in cases where the elemental composition analysis returned multiple options. About 85% of the signals were elementally resolved by the $C_xH_yO_z$ formula in ambient air mass spectra. A small number of nitrogen containing compounds, such as nitroaromatics, were also identified but not included in the following analysis. Throughout of the context, we use the word "species" to refer to all compounds with assigned molecular formula, which may include multiple isomers.

2.3. Complementary measurements

In addition to CHARON-PTR-ToF-MS, a Thermal desorption Aerosol Gas chromatograph (TAG) was also employed to measure a series of particle-phase organic species. Details of the TAG operation and data analysis protocols can be found in previous studies (He et al., 2020; Wang et al., 2020b; Zhu et al., 2021). The elemental composition and mass concentration of particles were measured by an Aerodyne high-resolution time-of-flight Aerosol Mass Spectrometer (AMS), with details of operation and quality control protocols given by our recent

268 study (Huang et al., 2021). Volatile organic compounds (VOCs, $C_2 - C_{12}$) were analyzed by a

269 custom-built online gas chromatography system equipped with a mass spectrometer and a flame

270 ionization detector (GC-MS/FID). The performance of this system can be found in our previous

271 publications (Zhu et al., 2018; Wang et al., 2014). Meteorological parameters (ambient

272 temperature, wind speed, wind direction, and relative humidity) were collected by an automatic

273 weather station (Metone 590 series) mounted on the roof top of the campaign site.

274 **2.4. Gas-particle partitioning measurements vs. modeling**

275 The CHARON-PTR-ToF-MS measured gas- and particle-phase concentrations of a given

276 species i can be used to calculate its particle-phase fraction ($F_{p,i}$).

277
$$P_i = \frac{\frac{I_{p,i} \times \left(\frac{m}{z_i} - 1\right)}{V_m \times S_i}}{EF} \tag{6}$$

278
$$G_i = \frac{I_{g,i} \times \left(\frac{m}{z_i} - 1\right)}{V_m \times S_i} \tag{7}$$

279
$$F_{p,i} = \frac{P_i}{P_i + G_i} \tag{8}$$

280 where P_i and G_i are the mass concentrations (ng m^{-3}) of species i in the particle and gas

281 phase, respectively. $I_{p,i}$ and $I_{g,i}$ are the normalized signal (ncps) of the PTR-ToF-MS detected

282 ion i in the particle and gas phase, respectively. V_m is taken as 22.4 L/mol. S_i is calculated

283 or measured sensitivity (ncps ppb^{-1}), see details in Section 2.2.3. As structural isomers cannot

284 be resolved in the mass spectra, the calculation here assumes that all isomers with the same

285 molecular formula have the same chemical properties, i.e., saturation vapor pressures.

286 Substitution of Equations (6) and (7) to Equation (8) yields the final expression of the particle-

287 phase fraction of species i ($F_{p,i}$), which is a function of the observed PTR-MS raw signals of

288 species i in the gas and particle phase (in total ion counts), as well as the particle enrichment

289   factor (EF) of species i.

$$F_{p,i} = \frac{I_{p,i}/EF}{I_{p,i}/EF + I_{g,i}} \tag{9}$$

291   Gas-particle partitioning of a given analyte i was also modeled using the equilibrium

292   partitioning theory (Pankow, 1994):

$$F_{p,i} = \frac{1}{1 + C_i^* / C_{OA}} \tag{10}$$

$$C_i^* = \frac{10^6 Mw_i \zeta_i p_i}{RT} \tag{11}$$

295   where C_{OA} is the organic aerosol concentration measured by AMS ($\mu g\ m^{-3}$), C_i^* is the

296   saturation mass concentration ($\mu g\ m^{-3}$), Mw_i is the molecular weight ($g\ mol^{-1}$), ζ is the

297   activity coefficient (assumed as unity), p_i is the pure component liquid vapor pressure (Pa), R

298   is the universal gas constant ($8.2 \times 10^{-5}\ m^3\ atm\ K^{-1}\ mol^{-1}$), and T is the ambient temperature

299   (K). As detailed chemical information is lacking for all species detected by PTR-ToF-MS, here

300   we use the expression given by Donahue et al. (2011) to approximate the value of C_i^*:

$$\log_{10} C_i^* = (n_C^0 - n_C^i) b_C - n_O^i b_O - 2 \frac{n_C^i n_O^i}{n_C^i + n_O^i} b_{CO} \tag{12}$$

302   where $n_C^0 = 25$, $b_C = 0.475$, $b_O = 2.3$, and $b_{CO} = -0.3$.

303

2.5. Uncertainties in the measured and modeled gas-particle partitioning

305   The uncertainty associated with the PTR-MS measured concentrations in both gas and

306   particle phases is less than 15% for compounds with chemical standards based on the optimally

307   fitted transmission efficiency curve. For those in the absence of standards, their PTR

308   sensitivities were calculated theoretically using Equations (1-2), and the uncertainty in the

309   calculation mainly arises from the estimation of polarizability and dipole moment of the target

molecule, which has been estimated to be within ~ 50% when only the elemental composition of that molecule is given (Sekimoto et al., 2017). It is important to note, however, that the uncertainty associated with the estimated PTR sensitivity has zero influence on the measured particle-phase fraction of any given compound because the sensitivity term is essentially canceled in the divisor function in Equation (9). The uncertainty associated with the particle fraction of a given species i derived from the PTR-MS measurements arises predominantly from the "EF" term. Since the uncertainty of the measured EF depends on the uncertainty of $I_{p,i}$, we thus express the overall uncertainties of the measured gas-particle partitioning as:

$$Unc(F_{p,i})=\sqrt{Unc(EF)^2+Unc(I_{g,i})^2} \tag{13}$$

with the calibration standards used in this study, the enrichment factor is calculated to be within 25% error ($Unc(EF)$) (see detailed calculations listed in Table S2 and S3), including the effect of wall loss inside the inlet tubing and the precision of the measurement. Huang et al. (2019) has tested the uncertainty of wall loss ($Unc(I_{g,i})$) in this PTR-MS instrument as 28%. Therefore, the overall uncertainty in the measured particle-phase fraction ($Unc(F_{p,i})$) was estimated as 38%.

The uncertainty associated with the modeled gas-particle partitioning arises primarily from the uncertainty in the estimation of the saturation mass concentration (C_i^*) based on the method developed by Donahue et al. (2011). In this method, the saturation mass concentration of species i is a non-linear function of the numbers of carbon and oxygen atoms in that particular species, see Equation (12). For each generic molecular formula, i.e., C_xH_y, C_xH_yO, $C_xH_yO_2$, and $C_xH_yO_4$, Donahue et al. (2011) have used a total of 25, 48, 18, and 10 chemical standards with known volatilities to validate the estimated saturation concentrations, and the estimated errors

332 were taken as 34%, 16%, 25%, and 54%, respectively (see Table S6). As the $C_xH_yO_3$ group was

333 not tested, we tentatively assumed the associated errors as the same as the $C_xH_yO_4$ group. The

334 extent to which these uncertainties may affect the difference between measurements and model

335 results was discussed in detail in the Supporting Information (Fig. S10).

336

337 **3. Results and Discussion**

338 **3.1. Particle enrichment: effect of desorption temperature**

339 Thermal desorption as a common procedure used in the chemical characterization of

340 organic aerosols is often susceptible to fragmentation of non-refractory compounds. Due to the

341 high temperature used to evaporate particles collected, labile and large molecules are inevitably

342 subject to fragmentation, thereby introducing large uncertainties to the measured mass and

343 composition of the particulate organic compounds (Lopez-Hilfiker et al., 2015; Yatavelli et al.,

344 2012; Zhao et al., 2013). Thermal decomposition of oxidized organic compounds has been

345 observed at vaporizer temperature as low as 200 °C, the lowest temperature required to vaporize

346 OA as reported (Stark et al., 2017). While decreasing the vaporizer temperature is necessary to

347 maintain the intact structure of labile molecules, low temperature (e.g., 85 °C), however, might

348 fail to completely evaporate the collected particles into vapors, resulting in an underestimation

349 of the collected OA mass (Inomata et al., 2014). Here we performed a series of sensitivity tests

350 to identify the optimal vaporizer temperature in the CHARON inlet for the measurements of

351 organic compounds in the particle phase.

352 Prior to the temperature sensitivity test, we have validated that the particle enrichment

353 factor, also known as collection efficiency and defined as the ratio of the particle mass

354 concentration upstream to downstream of the aerodynamic lens, does not depend on the particle

size. As shown in Fig. 1a, the measured EF value for ammonium nitrate particles, detected as NO_2^+ produced from the nitric acid vapor, remains constant as ~ 15 in the 150 – 450 nm particle size range. The lower values in the 100 – 150 nm size range can be explained by the lower particle transmission efficiency in the gas phase denuder, e.g., 75% – 80% for 100 nm particles (Eichler et al., 2015). Also, particles below 150 nm are less efficiently concentrated in the subsampling flow after the aerodynamic lens. Therefore, we used the monodisperse particles generated from selected organic standards at 300 nm for the temperature sensitivity test.

A number of chemical standards that are representative of alcohols, carbonyls, and carboxylic acids and with the vapor pressure ranging from 10^{-14} to 10^{-1} Pa at 25 °C (taken from EPA EPI Suite (2012), see values given in Table S1) were used to generate organic aerosols, which, upon size selection at 300 nm, were directed to the CHARON inlet. Particle evaporation occurs downstream of the aerodynamic lens in the gas phase and on the tube and orifice surface to which submicron particles rapidly diffuse at ~ 8 mbar operating pressure. The thermal desorption unit was designed to ensure that ammonium sulfate particles (10^{-20} Pa) can be completely evaporated (Piel et al., 2019; Eichler et al., 2015). As the desorption temperature was varied from 70 °C to 140 °C, the intensities of all detected ions (including both parent and fragment ions) for each organic standard analyzed were stable within 15%, as shown in Fig. 1b. Also note that we did not observe any ions produced from decarboxylation and/or dehydration during the particle evaporation process. This is because the relative low operation temperature and the short heat exposure time could effectively limit any thermal dissociation of organic molecules. This demonstrates that the parent molecule fragmentation, if any, does not occur under the range of desorption temperature used in the CHARON inlet, but rather results from the ionic dissociation process in the PTR ionization chamber, see more discussions in Section

378   3.3. We therefore used the sum total of intensities of all major ions detected as the PTR-ToF-

379   MS response to a given organic standard analyzed. Fig. 1c shows that the derived enrichment

380   factors stay constant for all compounds investigated ($Mw \sim 160 - 230$ g/mol). The relative

381   signals of all fragment ions were stable over the range of the desorption temperature as shown

382   in Fig. 2. This suggests that the desorption temperature used here, even as low as 70 °C, is

383   sufficient to evaporate SVOCs (volatility $> 10^{-14}$ Pa at 25 °C), due to the low operating pressure

384   (~ 8 mbar) that significantly enhances the partitioning shift to the gas phase. One low volatility

385   compound, sucrose (Mw is 342 g/mol and vapor pressure is 4.69×10^{-14} Pa), has a slightly lower

386   enhancement factor compared with all the other organic standards tested. This is mainly due to

387   the intensive dehydration of the parent compound in the ionization chamber, and as a result,

388   only a few fragment ions were captured, resulting in a lower PTR response and thereby lower

389   EF value calculated from Equations (3-5). The EF values of sucrose also have much higher

390   standard deviations at all temperatures due to fragmentation (Table S3).

391
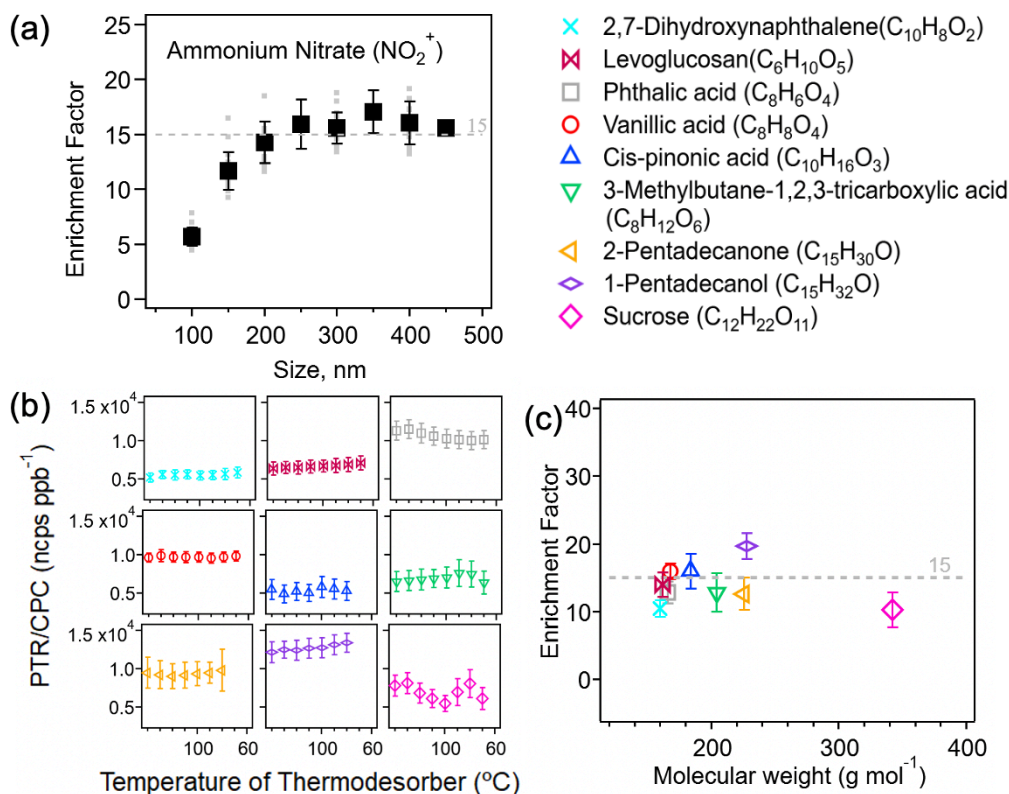
Figure 1. (a) Measured unitless enrichment factor (*EF*) of ammonium nitrate particles as a function of particle size in the 100 – 450 nm range. Grey markers represent all replicating measurements. The error bar denotes one standard deviation (1σ) of the average. (b) Ratios of PTR-ToF-MS signals (including both parent and fragment ions) to CPC counts (±1σ) at 300 nm for all organic standards studied. (c) *EF* (±1σ) of selected organic standards based on the calculated sensitivity.

398
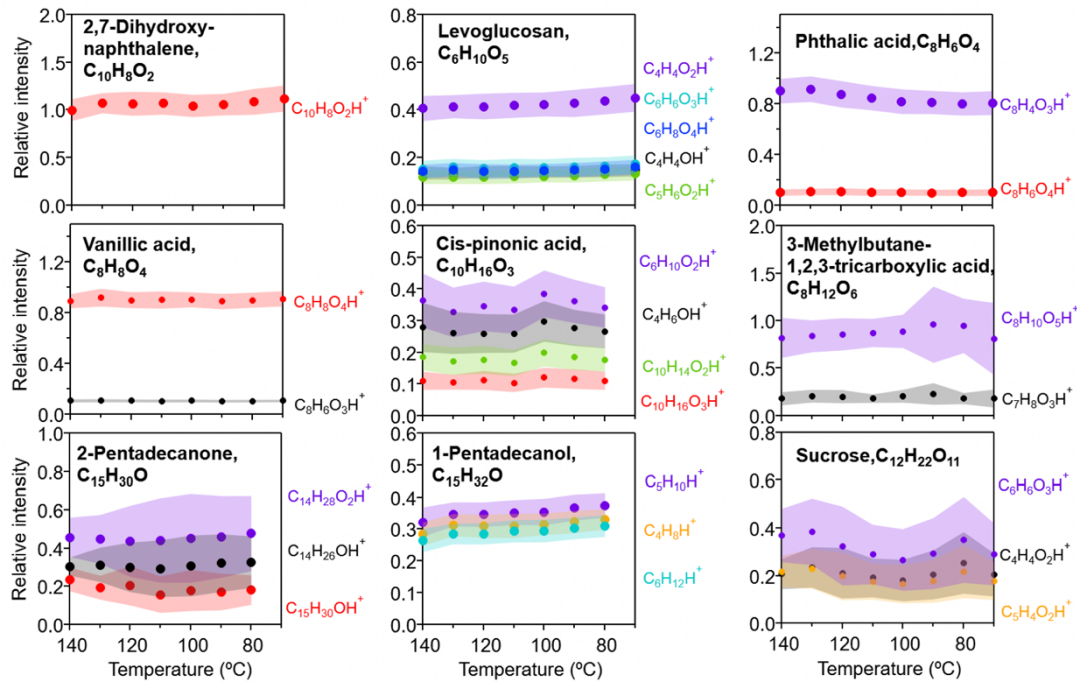
Figure 2. Ratios of CHARON-PTR-ToF-MS signals (ncps) to CPC measurements (ppb) of all detected ions (including both parents and fragments) for a given pure organic standard tested under different desorption temperatures (70 – 140 °C), normalized to the corresponding ratios obtained at 140 °C. Ions with relative intensities less than 10% are excluded. Red markers represent the parent peaks. Colored shades represent the relative standard deviations at different temperatures (exact values are given in Table S4).

It has been recognized that species with one functional group follow certain fragmentation patterns during the PTR ionization process (Pagonis et al., 2019; Francis et al., 2007; Spanel et al., 1997; Tani et al., 2003; Spanel and Smith, 1997), such as dehydration of acids and alcohols. The observed dissociation of carboxylic acid standards used in this study, e.g., phthalic acid and 3-methylbutane-1,2,3-tricarboxylic acid, can be explained by this common fragmentation

411　　pattern. The fragmentation mechanism of muti-functionalized species is rather complicated and

412　　a number of fragments can be produced upon PTR ionization. Nevertheless, the identity and

413　　abundance of fragments from a given muti-functionalized species have been found comparable

414　　under the same PTR operation protocols (Leglise et al., 2019; Gkatzelis et al., 2018a). For

415　　example, *cis*-pinonic acid yields the following fragments (main ions only and relative

416　　abundance in parentheses): *m/z* 71.049 (~28%), 115.075 (~36%), 167.108 (~19%), and 185.117

417　　(~11%), which is comparable with an earlier study (Leglise et al., 2019): *m/z* 71.049 (~27%),

418　　115.075 (~33%), 167.108 (~26%), and 185.117 (~14%) at 100 Td settings.

419

420　　**3.2. Molecular features of detected organic species**

421　　　A month-long field dataset of particle- and gas-phase organic species was collected at

422　　hourly resolution using the CHARON-PTR-ToF-MS instrument. A comparison of PTR-ToF-

423　　MS measurements with other techniques available on site was performed for both gas and

424　　particle phases. For the gas phase, quantitative measurements of a suite of VOCs by GC-

425　　MS/FID, including benzene, toluene, styrene, C_8 and C_9 aromatics, acrolein, and C_4, C_5, and C_6

426　　ketones, agree well with corresponding PTR-ToF-MS measurements, as shown in Fig. S6. For

427　　the particle phase, the time series of a group of $C_xH_yO_4$ species (including $C_4H_6O_4$, $C_5H_8O_4$,

428　　$C_6H_{10}O_4$, and $C_8H_6O_4$) are in reasonable agreement with corresponding measurements taken by

429　　TAG (r ~ 0.60 – 0.80), although the CHARON-PTR-ToF-MS measured total molecular mass

430　　is generally lower than the TAG measurements by a factor of 2 to 6 (Fig. S7). This is likely

431　　caused by the fragmentation (e.g., loss of H_2O, see Fig. S8) of the parent compounds during the

432　　ionization process, as discussed in detail in Section 3.3. The time series of total OA mass

433　　characterized by CHARON-PTR-ToF-MS also agree with the AMS measurements (r ~ 0.91,

434   Fig. S9). Previous studies have reported the particulate organics measured by PTR-MS with a

435   thermal desorption inlect account for 25% – 60% mass of the total organic aerosols measured

436   by AMS (Holzinger et al., 2013). Direct comparison of the total OA mass loading is not

437   applicable here since the CHARON-PTR-ToF-MS measurement only focused on compounds

438   with the mass to charge ratio below 300 Th. That the majority of ions detected by PTR are

439   present in the lower mass range is primarily due to the fragmentation of larger masses during

440   the ionization process, as discussed extensively in Section 3.3.
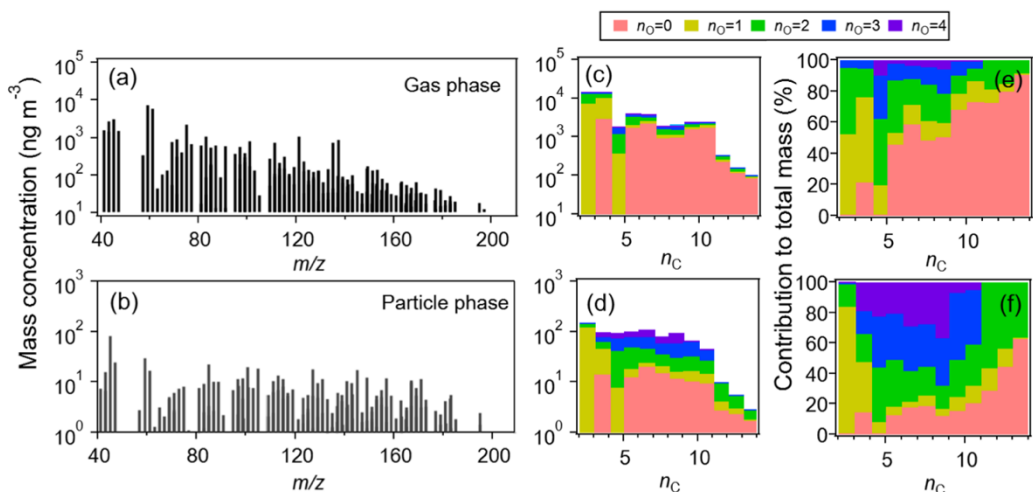

441

442   Figure 3. Background subtracted monthly-average PTR-ToF-MS mass spectra in the (a) gas

443   phase and (b) particle phase. Mass distributions of all identified species resolved by the carbon

444   and oxygen numbers (n_C and n_O) in the (c) gas phase and (d) particle phase, as well as their

445   relative contribution to the total organic mass in the (e) gas phase and (f) particle phase.

446

447   Fig. 3 (a-b) shows the PTR-ToF-MS spectra of dominant ions averaged over the entire

448   campaign in both gas and particle phases. The mass concentrations of individual ions are in the

449   range of 7.9 – 7179.3 ng m^{-3} in the gas phase and 0.6 – 82.7 ng m^{-3} in the particle phase. A total

450   of 152 species (with > 60% data points above the PTR-ToF-MS detection limits) are identified,

451   contributing to ~ 69% and ~ 44%, respectively, of the total organic mass measured in the gas

452   and particle phase. The molecular distribution characterized by the carbon and oxygen of these

453   species is given in Fig. 3 (c-d). The most abundant species are characterized by a generic

454   formula of C_xH_yO and $C_xH_yO_2$, resolving ~ 64% and ~ 46% in total of all identified species in

455   the gas and particle phase, respectively. Another dominant component in the gas phase is

456   hydrocarbon-like compounds (C_xH_y) (~ 27%), which contribute ~ 12% of the organic mass in

457   the particle phase. Species with higher oxygen numbers (> 2) contribute to a large fraction (~

458   42%) of the total particulate mass. These $C_xH_yO_{1-4}$ groups exhibit different diurnal cycles, as

459   shown in Fig. 4, reflecting their unique formation chemistry. The C_xH_y group peaks in the early

460   morning rush hour and likely originates from primary traffic emissions. On the contrary, both

461    $C_xH_yO_3$ and $C_xH_yO_4$ groups peak at noon, suggesting a strong secondary formation source. The

462   diurnal trends for C_xH_yO and $C_xH_yO_2$ groups are relatively flat during the day, likely indicative

463   of an intertwined primary emission and secondary formation processes.

464
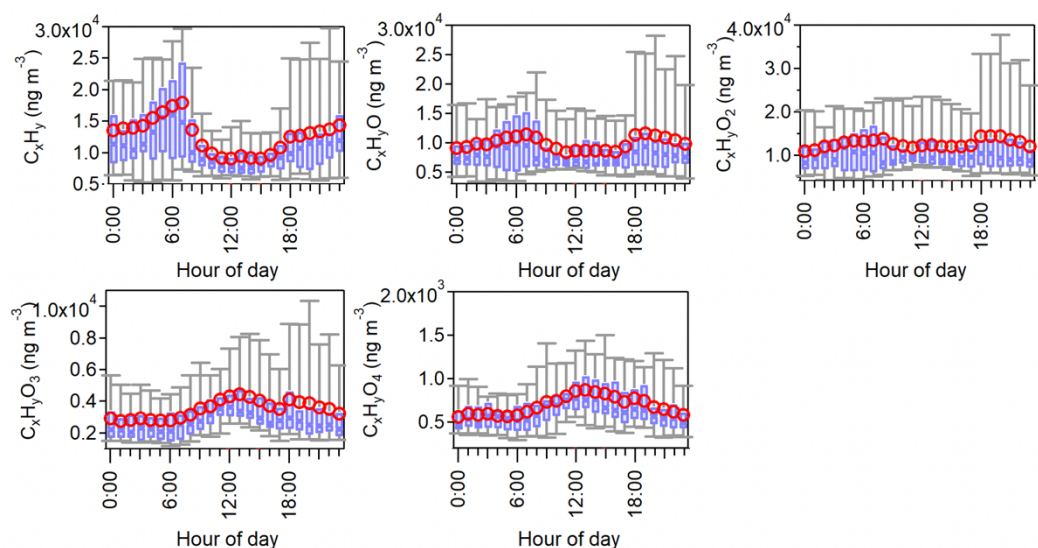
465

466 Figure 4. Diurnal variations of observed gas-phase species with a generic formula of $C_{2-13}H_{2-}$

467 $_{22}O_{0-4}$. Hourly average values (ng m^{-3}), together with 10th, 25th, 75th, and 90th percentiles, are

468 also plotted.

469

470 **3.3. Measured vs. modeled gas-particle partitioning**

471 Fig. 5 shows the calculated particle-phase fraction (F_p) of the identified 152 species using

472 the CHARON-PTR-ToF-MS measurements in both phases. It is important to note that an

473 authentic standard is not required for the calculation of F_p for any given species, because the

474 PTR sensitivity term is essentially canceled in the divisor function in Equations (6-8). Also

475 given in Fig. 5 is the simulated F_p of the derived molecular formulas of all species identified

476 using the equilibrium partitioning theory, see method described in Section 2.4. Interestingly,

477 for oxidized species such as $C_xH_yO_4$, their measured F_p agree reasonably with the simulations,

478 as shown in Fig. 5a. The $C_xH_yO_4$ group resides in the relatively higher mass range, and species

24

479 identified in this group are more likely actual compounds rather than fragments from larger

480 parent molecules. Even these species dessociate into lower mass ions during PTR ionization,

481 their calculated particle-phase fractions are unaffected by such fragmentation processes because

482 signals of parent ions decrease by the same extent upon fragmentation in both gas and particle

483 phases. As the oxygen number decreases, the measured F_p values tend to deviate from the

484 simulations by up to several orders of magnitude. Note that these less oxidized compounds (e.g.,

485 C_xH_y) are mostly small molecules and they are highly unlikely present in the condensed phase

486 as closed-shell monomers (Pankow and Asher, 2008; Holzinger et al., 2010). Instead, they are

487 more likely fragments produced from the decomposition of larger molecules, which no

488 surprisingly favor partitioning in the particle phase. It is worth noting that the uptake of small

489 oxidized compounds on the aerosol aqueous phase does not significantly affect the overall

490 particle phase fraction of these compounds, see detailed calculations in Text S3. The

491 discrepancy in the measurement-model comparison underscores the importance of

492 understanding the fragmentation mechanism during PTR ionization when extracting molecular

493 features from the raw mass spectra.

494   Parent ion fragmentation has been widely observed in PTR-MS instruments (Pagonis et al.,

495 2019). Oxygenates exhibit trends in neutral losses of water or saturated alcohols. Here, we

496 apply a correction to the molecular formula of the 152 identified species by assuming that these

497 species are fragments produced from their parent precursors through the neutral losses of a

498 carboxyl group ($-CO_2$), a carbonyl group ($-CO$), a hydroxyl group ($-H_2O$), or an alcohol group

499 ($-C_2H_6O$). By applying this correction, the modeled F_p of a given species $C_xH_yO_z$ would actually

500 represent the particle-phase fraction of the its parent species $C_xH_yO_z \cdot CO_2$, $C_xH_yO_z \cdot CO$,

501 $C_xH_yO_z \cdot H_2O$, or $C_xH_yO_z \cdot C_2H_6O$. As shown in Fig. 5 (b-e), such a correction could significantly

502 increase the modeled F_p values by several orders of magnitude. The assumption of neutral

503 losses of CO_2 or C_2H_6O allows for much improved agreement between modeled vs. measured

504 F_p values for less oxidized species. This implies that these small and less oxidized species are

505 likely fragments resulting from the decomposition of larger parent precursors. As our particle

506 enrichment test (details given in Section 3.1) has confirmed that the thermal desorption

507 temperature employed for particle evaporation does not lead to any intensive fragmentation,

508 therefore the collision-induced dissociation during the proton transfer reaction process becomes

509 the predominant process that produces fragments (Lindinger et al., 1998; Gueneron et al., 2015;

510 Gkatzelis et al., 2018b). Although the electric field applied to the drift tube is considered low

511 to moderate compared with most previous PTR-MS measurements ($E/N \sim 100$ Td in this study

512 vs. $E/N \sim 120 - 140$ Td commonly found in PTR-MS measurements) (Pagonis et al., 2019),

513 parent ion fragmentation was still widely observed here and complicated the mass spectra

514 interpretation and molecular feature extraction. While some recent CHARON measurements

515 employed lower electric field in the drift tube ($E/N \sim 60$ Td) (Leglise et al., 2019; Gkatzelis et

516 al., 2018a; Piel et al., 2019), such conditions could promote the formation of water cluster ions,

517 which increase with humidity and reduce the PTR sensitivity, and therefore are not ideally

518 suitable for our field measurements. A compromise solution would be using a moderate electric

519 field in the drift tube (e.g., ~ 100 Td) and meanwhile applying appropriate molecular corrections

520 to all ions detected in the mass spectra by considering possible neutral losses of small moieties.

521 Since in this study only the information of molecular formula is derived from the PTR-MS

522 spectra, we thus provide the lower and upper bound of the gas-particle partitioning corrections

523 owing to neutral losses of H_2O and CO_2, respectively. In general, lower masses with higher

524 volatilities are subject to notable changes in the particle-phase fraction as a result of neutral

525 losses during the PTR ionization process, see detailed discussions in Text S2.

526

527
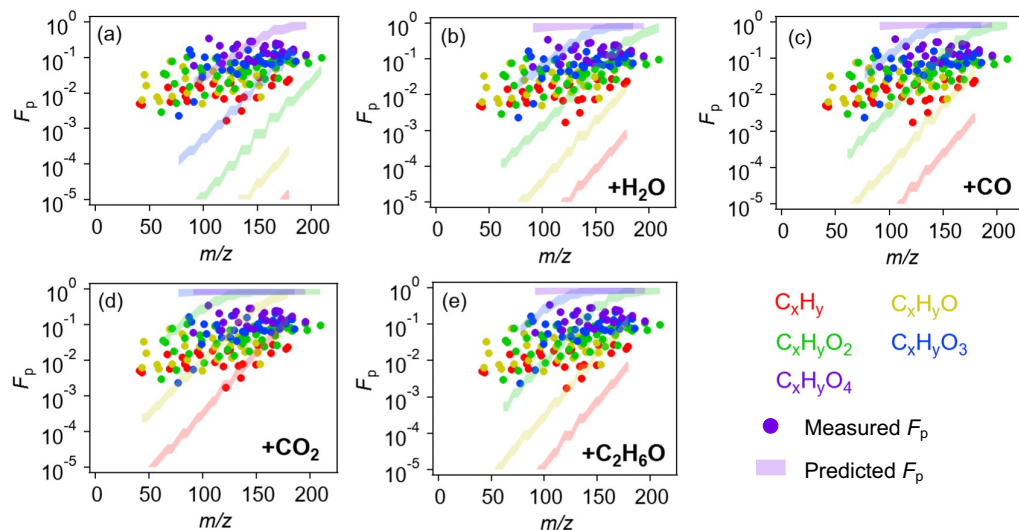
Figure 5. (a) Campaign average fraction of organic species in the particle phase (F_p) grouped by the oxygen number. Solid markers represent the calculated F_p based on the CHARON-PTR-ToF-MS measurements. Colored shades represent the predicted F_p of corresponding molecular formulas. (b-e) Measured vs. predicted F_p assuming the identified species are fragments of corresponding parent compounds through neutral losses of H_2O, CO, CO_2, and C_2H_6O, respectively (values are given in Table S5).

534

4. Conclusions

536　　Recent studies have suggested that some of the model-measurement discrepancies in the representation of ambient organic aerosol budget might be due to the nonequilibrium gas/particle partitioning caused by kinetic limitations in the presence of glassy or semi-solid phase (Perraud et al., 2012; Mai et al., 2015; Shiraiwa et al., 2013). It is therefore necessary to

540   validate whether the equilibrium partitioning theory could adequately describe the

541   condensation of semivolatile organic vapors onto atmospheric aerosols under ambient

542   conditions, and the accurate measurement of these SVOCs in both gas and particle phases is

543   the crucial prerequisite. In this study, we have employed the PTR-ToF-MS instrument coupled

544   to a CHARON inlet, together with a suite of complementary measurements, to characterize the

545   atmospheric partitioning behaviors of an array of SVOCs in an urban environment of East

546   China. Prior to the application to the field measurements, we first performed a series of

547   laboratory experiments to test whether the CHARON inlet is capable of sampling organic

548   molecules (including alcohols, carbonyls, and carboxylic acids) in their native states. With the

549   low pressure condition used in the CHARON inlet, a thermal desorption temperature less than

550   140 °C could adequately evaporate organic compounds with vapor pressure higher than 10^{-14}

551   Pa while minimizing the thermal decomposition of labile functionalities. The auto-switch

552   function between the gas and particle mode with one single PTR-ToF-MS instrument could

553   monitor gaseous and particulate organic compounds in real time, thereby providing important

554   information of their partitioning behaviors in the ambient atmosphere. Particle-phase fractions

555   of a total of 152 organic species were derived from the CHARON-PTR-ToF-MS measurements

556   and further compared with model predictions using the instantaneous equilibrium partitioning

557   theory. While the model captured the particle-phase fraction of oxidized compounds (e.g.,

558     $C_xH_yO_{3-4}$), predictions of less oxidized compounds, notably the C_xH_y family, differ from the

559   corresponding measurements by several orders of magnitude. Such a large discrepancy is very

560   likely caused by the intensive fragmentation of the parent organic compounds during the PTR

561   ionization process. Accounting for common fragmentation patterns in the simulations of gas-

562   particle partitioning, for example, neutral losses of $-CO_2$, $-CO$, $-H_2O$, or $-C_2H_6O$, could largely

28

improve the model-measurement agreement. Such corrections are very necessary towards an accurate measurement of both particle- and gas-phase SVOCs using the CHARON-PTR-ToF-MS instrument. Our study suggests the crucial importance of optimizing operation conditions and understanding the fragmentation mechanism in the particle collection, vaporization, and ionization processes in understanding the gas-particle partitioning of organic compounds using any thermal desorption based aerosol measurement method.

References

Antonsen, S., Bunkan, A. J. C., D'Anna, B., Eichler, P., Farren, N., Hallquist, M., Hamilton, J. F., Kvarnliden, H., Mikoviny, T., Muller, M., Nielsen, C. J., Stenstrom, Y., Tan, W., Wisthaler,

A., and Zhu, L.: Atmospheric chemistry of tert-butylamine and AMP, in: Enrgy Proced, edited by: Dixon, T., Laloui, L., and Twinning, S., Energy Procedia, Elsevier Science Bv, Amsterdam, 1026-1032, 10.1016/j.egypro.2017.03.1248, 2017.

Crounse, J. D., McKinney, K. A., Kwan, A. J., and Wennberg, P. O.: Measurement of gas-phase hydroperoxides by chemical ionization mass spectrometry, Anal. Chem., 78, 6726-6732, 10.1021/ac0604235, 2006.

de Gouw, J. and Warneke, C.: Measurements of volatile organic compounds in the earths atmosphere using proton-transfer-reaction mass spectrometry, Mass Spectrometry Reviews, 26, 223-257, 10.1002/mas.20119, 2007.

Donahue, N. M., Epstein, S. A., Pandis, S. N., and Robinson, A. L.: A two-dimensional volatility basis set: 1. organic-aerosol mixing thermodynamics, Atmos. Chem. Phys., 11, 3303-3318, 10.5194/acp-11-3303-2011, 2011.

Eichler, P., Muller, M., D'Anna, B., and Wisthaler, A.: A novel inlet system for online chemical analysis of semi-volatile submicron particulate matter, Atmos. Meas. Tech., 8, 1353-1360, 10.5194/amt-8-1353-2015, 2015.

Eichler, P., Muller, M., Rohmann, C., Stengel, B., Orasche, J., Zimmermann, R., and Wisthaler, A.: Lubricating Oil as a Major Constituent of Ship Exhaust Particles, Environ. Sci. Technol. Lett., 4, 54-58, 10.1021/acs.estlett.6b00488, 2017.

EPA: Estimation Program Interface (EPI) Suite (v4.11), US [code], 2012.

Francis, G. J., Milligan, D. B., and McEwan, M. J.: Gas-Phase Reactions and Rearrangements of Alkyl Esters with H3O+, NO+, and O2•+: A Selected Ion Flow Tube Study, J. Phys. Chem. A, 111, 9670-9679, 10.1021/jp0731304, 2007.

Gkatzelis, G. I., Tillmann, R., Hohaus, T., Muller, M., Eichler, P., Xu, K. M., Schlag, P., Schmitt, S. H., Wegener, R., Kaminski, M., Holzinger, R., Wisthaler, A., and Kiendler-Scharr, A.: Comparison of three aerosol chemical characterization techniques utilizing PTR-ToF-MS: a study on freshly formed and aged biogenic SOA, Atmos. Meas. Tech., 11, 1481-1500, 2018a.

Gkatzelis, G. I., Hohaus, T., Tillmann, R., Gensch, I., Muller, M., Eichler, P., Xu, K. M., Schlag, P., Schmitt, S. H., Yu, Z. J., Wegener, R., Kaminski, M., Holzinger, R., Wisthaler, A., and Kiendler-Scharr, A.: Gas-to-particle partitioning of major biogenic oxidation products: a study

on freshly formed and aged biogenic SOA, Atmos. Chem. Phys., 18, 12969-12989, 10.5194/acp-18-12969-2018, 2018b.

Gueneron, M., Erickson, M. H., VanderSchelden, G. S., and Jobson, B. T.: PTR-MS fragmentation patterns of gasoline hydrocarbons, International Journal of Mass Spectrometry, 379, 97-109, 10.1016/j.ijms.2015.01.001, 2015.

He, X., Wang, Q., Huang, X. H. H., Huang, D. D., Zhou, M., Qiao, L., Zhu, S., Ma, Y.-g., Wang, H.-l., Li, L., Huang, C., Xu, W., Worsnop, D. R., Goldstein, A. H., and Yu, J. Z.: Hourly measurements of organic molecular markers in urban Shanghai, China: Observation of enhanced formation of secondary organic aerosol during particulate matter episodic periods, Atmos. Environ., 240, 10.1016/j.atmosenv.2020.117807, 2020.

Heald, C. L. and Kroll, J. H.: The fuel of atmospheric chemistry: Toward a complete description of reactive organic carbon, Sci. Adv., 6, 10.1126/sciadv.aay8967, 2020.

Holzinger, R., Goldstein, A. H., Hayes, P. L., Jimenez, J. L., and Timkovsky, J.: Chemical evolution of organic aerosol in Los Angeles during the CalNex 2010 study, Atmos. Chem. Phys., 13, 10125-10141, 10.5194/acp-13-10125-2013, 2013.

Holzinger, R., Williams, J., Herrmann, F., Lelieveld, J., Donahue, N. M., and Rockmann, T.: Aerosol analysis using a Thermal-Desorption Proton-Transfer-Reaction Mass Spectrometer (TD-PTR-MS): a new approach to study processing of organic aerosols, Atmos. Chem. Phys., 10, 2257-2267, 10.5194/acp-10-2257-2010, 2010.

Holzinger, R., Acton, W. J. F., Bloss, W. J., Breitenlechner, M., Crilley, L. R., Dusanter, S., Gonin, M., Gros, V., Keutsch, F. N., Kiendler-Scharr, A., Kramer, L. J., Krechmer, J. E., Languille, B., Locoge, N., Lopez-Hilfiker, F., Materić, D., Moreno, S., Nemitz, E., Quéléver, L. L. J., Sarda Esteve, R., Sauvage, S., Schallhart, S., Sommariva, R., Tillmann, R., Wedel, S., Worton, D. R., Xu, K., and Zaytsev, A.: Validity and limitations of simple reaction kinetics to calculate concentrations of organic compounds from ion counts in PTR-MS, Atmos. Meas. Tech., 12, 6193-6208, 10.5194/amt-12-6193-2019, 2019.

Huang, D. D., Zhu, S., An, J., Wang, Q., Qiao, L., Zhou, M., He, X., Ma, Y., Sun, Y., Huang, C., Yu, J. Z., and Zhang, Q.: Comparative Assessment of Cooking Emission Contributions to Urban Organic Aerosol Using Online Molecular Tracers and Aerosol Mass Spectrometry Measurements, Environ. Sci. Technol., 10.1021/acs.est.1c03280, 2021.

645   Huang, G., Liu, Y., Shao, M., Li, Y., Chen, Q., Zheng, Y., Wu, Z., Liu, Y., Wu, Y., Hu, M., Li,
646   X., Lu, S., Wang, C., Liu, J., Zheng, M., and Zhu, T.: Potentially Important Contribution of
647   Gas-Phase Oxidation of Naphthalene and Methylnaphthalene to Secondary Organic Aerosol
648   during Haze Events in Beijing, Environ. Sci. Technol., 53, 1235-1244, 10.1021/acs.est.8b04523,
649   2019.

650   Inomata, S., Sato, K., Hirokawa, J., Sakamoto, Y., Tanimoto, H., Okumura, M., Tohno, S., and
651   Imamura, T.: Analysis of secondary organic aerosols from ozonolysis of isoprene by proton
652   transfer reaction mass spectrometry, Atmos. Environ., 97, 397-405,
653   10.1016/j.atmosenv.2014.03.045, 2014.

654   Krechmer, J. E., Groessl, M., Zhang, X., Junninen, H., Massoli, P., Lambe, A. T., Kimmel, J.
655   R., Cubison, M. J., Graf, S., Lin, Y.-H., Budisulistiorini, S. H., Zhang, H., Surratt, J. D.,
656   Knochenmuss, R., Jayne, J. T., Worsnop, D. R., Jimenez, J.-L., and Canagaratna, M. R.: Ion
657   mobility spectrometry–mass spectrometry (IMS–MS) for on- and offline analysis of
658   atmospheric gas and aerosol species, Atmos. Meas. Tech., 9, 3245-3262, 10.5194/amt-9-3245-
659   2016, 2016.

660   Le Breton, M., Wang, Y. J., Hallquist, A. M., Pathak, R. K., Zheng, J., Yang, Y. D., Shang, D.
661   J., Glasius, M., Bannan, T. J., Liu, Q. Y., Chan, C. K., Percival, C. J., Zhu, W. F., Lou, S. R.,
662   Topping, D., Wang, Y. C., Yu, J. Z., Lu, K. D., Guo, S., Hu, M., and Hallquist, M.: Online gas-
663   and particle-phase measurements of organosulfates, organosulfonates and nitrooxy
664   organosulfates in Beijing utilizing a FIGAERO ToF-CIMS, Atmos. Chem. Phys., 18, 10355-
665   10371, 2018.

666   Lee, B. H., Lopez-Hilfiker, F. D., D'Ambro, E. L., Zhou, P., Boy, M., Petäjä, T., Hao, L.,
667   Virtanen, A., and Thornton, J. A.: Semi-volatile and highly oxygenated gaseous and particulate
668   organic compounds observed above a boreal forest canopy, Atmos. Chem. Phys., 18, 11547-
669   11562, 10.5194/acp-18-11547-2018, 2018.

670   Leglise, J., Muller, M., Piel, F., Otto, T., and Wisthaler, A.: Bulk Organic Aerosol Analysis by
671   Proton-Transfer-Reaction Mass Spectrometry: An Improved Methodology for the
672   Determination of Total Organic Mass, O:C and H:C Elemental Ratios, and the Average
673   Molecular Formula, Anal. Chem., 91, 12619-12624, 10.1021/acs.analchem.9b02949, 2019.

674   Lindinger, W., Hansel, A., and Jordan, A.: Proton-transfer-reaction mass spectrometry (PTR-
675   MS): on-line monitoring of volatile organic compounds at pptv levels, Chem. Soc. Rev., 27,

347-354, 10.1039/a827347z, 1998.

Lopez-Hilfiker, F. D., Mohr, C., Ehn, M., Rubach, F., Kleist, E., Wildt, J., Mentel, T. F., Lutz, A., Hallquist, M., Worsnop, D., and Thornton, J. A.: A novel method for online analysis of gas and particle composition: description and evaluation of a Filter Inlet for Gases and AEROsols (FIGAERO), Atmos. Meas. Tech., 7, 983-1001, 10.5194/amt-7-983-2014, 2014.

Lopez-Hilfiker, F. D., Mohr, C., Ehn, M., Rubach, F., Kleist, E., Wildt, J., Mentel, T. F., Carrasquillo, A. J., Daumit, K. E., Hunter, J. F., Kroll, J. H., Worsnop, D. R., and Thornton, J. A.: Phase partitioning and volatility of secondary organic aerosol components formed from α-pinene ozonolysis and OH oxidation: the importance of accretion products and other low volatility compounds, Atmos. Chem. Phys., 15, 7765-7776, 10.5194/acp-15-7765-2015, 2015.

Lopez-Hilfiker, F. D., Mohr, C., D'Ambro, E. L., Lutz, A., Riedel, T. P., Gaston, C. J., Iyer, S., Zhang, Z., Gold, A., Surratt, J. D., Lee, B. H., Kurten, T., Hu, W. W., Jimenez, J., Hallquist, M., and Thornton, J. A.: Molecular Composition and Volatility of Organic Aerosol in the Southeastern U.S.: Implications for IEPOX Derived SOA, Environ. Sci. Technol., 50, 2200-2209, 10.1021/acs.est.5b04769, 2016.

Lutz, A., Mohr, C., Le Breton, M., Lopez-Hilfiker, F. D., Priestley, M., Thornton, J. A., and Hallquist, M.: Gas to Particle Partitioning of Organic Acids in the Boreal Atmosphere, ACS Earth Space Chem., 3, 1279-1287, 10.1021/acsearthspacechem.9b00041, 2019.

Mai, H., Shiraiwa, M., Flagan, R. C., and Seinfeld, J. H.: Under What Conditions Can Equilibrium Gas-Particle Partitioning Be Expected to Hold in the Atmosphere?, Environ. Sci. Technol., 49, 11485-11491, 10.1021/acs.est.5b02587, 2015.

Muller, M., Eichler, P., D'Anna, B., Tan, W., and Wisthaler, A.: Direct Sampling and Analysis of Atmospheric Particulate Organic Matter by Proton-Transfer-Reaction Mass Spectrometry, Anal. Chem., 89, 10889-10897, 10.1021/acs.analchem.7b02582, 2017.

Pagonis, D., Sekimoto, K., and de Gouw, J.: A Library of Proton-Transfer Reactions of H3O+ Ions Used for Trace Gas Detection, Journal of the American Society for Mass Spectrometry, 30, 1330-1335, 10.1007/s13361-019-02209-3, 2019.

Palm, B. B., Peng, Q. Y., Fredrickson, C. D., Lee, B., Garofalo, L. A., Pothier, M. A., Kreidenweis, S. M., Farmer, D. K., Pokhrel, R. P., Shen, Y. J., Murphy, S. M., Permar, W., Hu, L., Campos, T. L., Hall, S. R., Ullmann, K., Zhang, X., Flocke, F., Fischer, E. V., and Thornton,

706   J. A.: Quantification of organic aerosol and brown carbon evolution in fresh wildfire plumes,
707   Proc Natl Acad Sci U S A, 117, 29469-29477, 10.1073/pnas.2012218117, 2020.

708   Pankow, J. F.: An absorption-model of the gas aerosol partitioning involved in the formation of
709   secondary organic aerosol, Atmos. Environ., 28, 189-193, 10.1016/1352-2310(94)90094-9,
710   1994.

711   Pankow, J. F. and Asher, W. E.: SIMPOL.1: a simple group contribution method for predicting
712   vapor pressures and enthalpies of vaporization of multifunctional organic compounds, Atmos.
713   Chem. Phys., 8, 2773-2796, 10.5194/acp-8-2773-2008, 2008.

714   Peng, Y., Wang, H., Wang, Q., Jing, S., An, J., Gao, Y., Huang, C., Yan, R., Dai, H., Cheng, T.,
715   Zhang, Q., Li, M., Hu, J., Shi, Z., Li, L., Lou, S., Tao, S., Hu, Q., Lu, J., and Chen, C.:
716   Observation-based sources evolution of non-methane hydrocarbons (NMHCs) in a megacity of
717   China, J. Environ. Sci., 124, 794-805, 10.1016/j.jes.2022.01.040, 2023.

718   Perraud, V., Bruns, E. A., Ezell, M. J., Johnson, S. N., Yu, Y., Alexander, M. L., Zelenyuk, A.,
719   Imre, D., Chang, W. L., Dabdub, D., Pankow, J. F., and Finlayson-Pitts, B. J.: Nonequilibrium
720   atmospheric secondary organic aerosol formation and growth, Proc Natl Acad Sci U S A, 109,
721   2836-2841, 10.1073/pnas.1119909109, 2012.

722   Piel, F., Muller, M., Mikoviny, T., Pusede, S. E., and Wisthaler, A.: Airborne measurements of
723   particulate organic matter by proton-transfer-reaction mass spectrometry (PTR-MS): a pilot
724   study, Atmos. Meas. Tech., 12, 5947-5958, 10.5194/amt-12-5947-2019, 2019.

725   Piel, F., Müller, M., Winkler, K., Skytte af Sätra, J., and Wisthaler, A.: Introducing the extended
726   volatility range proton-transfer-reaction mass spectrometer (EVR PTR-MS), Atmos. Meas.
727   Tech., 14, 1355-1363, 10.5194/amt-14-1355-2021, 2021.

728   Sekimoto, K., Li, S. M., Yuan, B., Koss, A., Coggon, M., Warneke, C., and de Gouw, J.:
729   Calculation of the sensitivity of proton-transfer-reaction mass spectrometry (PTR-MS) for
730   organic trace gases using molecular properties, International Journal of Mass Spectrometry, 421,
731   71-94, 10.1016/j.ijms.2017.04.006, 2017.

732   Shiraiwa, M. and Seinfeld, J. H.: Equilibration timescale of atmospheric secondary organic
733   aerosol partitioning, Geophysical Research Letters, 39, n/a-n/a, 10.1029/2012gl054008, 2012.

734   Shiraiwa, M., Zuend, A., Bertram, A. K., and Seinfeld, J. H.: Gas-particle partitioning of

735 atmospheric aerosols: interplay of physical state, non-ideal mixing and morphology, Phys.
736 Chem. Chem. Phys., 15, 11441-11453, 10.1039/c3cp51595h, 2013.

737 Spanel, P. and Smith, D.: SIFT studies of the reactions of H3O+, NO+ and O2+ with a series
738 of   alcohols,   Int.   J.   Mass   Spectrom.   Ion   Processes,   167-168,   375-388,
739 https://doi.org/10.1016/S0168-1176(97)00085-2, 1997.

740 Spanel, P., Ji, Y. F., and Smith, D.: SIFT studies of the reactions of H3O+, NO+ and O-2(+)
741 with a series of aldehydes and ketones, International Journal of Mass Spectrometry, 165, 25-
742 37, 10.1016/s0168-1176(97)00166-3, 1997.

743 Stark, H., Yatavelli, R. L. N., Thompson, S. L., Kang, H., Krechmer, J. E., Kimmel, J. R., Palm,
744 B. B., Hu, W. W., Hayes, P. L., Day, D. A., Campuzano-Jost, P., Canagaratna, M. R., Jayne, J.
745 T., Worsnop, D. R., and Jimenez, J. L.: Impact of Thermal Decomposition on Thermal
746 Desorption Instruments: Advantage of Thermogram Analysis for Quantifying Volatility
747 Distributions   of   Organic   Species,   Environ.   Sci.   Technol.,   51,   8491-8500,
748 10.1021/acs.est.7b00160, 2017.

749 Tan, W., Zhu, L., Mikoviny, T., Nielsen, C. J., Wisthaler, A., Eichler, P., Muller, M., D'Anna,
750 B., Farren, N. J., Hamilton, J. F., Pettersson, J. B. C., Hallquist, M., Antonsen, S., and Stenstrom,
751 Y.: Theoretical and Experimental Study on the Reaction of tert-Butylamine with OH Radicals
752 in the Atmosphere, J. Phys. Chem. A, 122, 4470-4480, 10.1021/acs.jpca.8b01862, 2018.

753 Tani, A., Hayward, S., and Hewitta, C. N.: Measurement of monoterpenes and related
754 compounds by proton transfer reaction-mass spectrometry (PTR-MS), International Journal of
755 Mass Spectrometry, 223, 561-578, 10.1016/s1387-3806(02)00880-1, 2003.

756 Thompson, S. L., Yatavelli, R. L. N., Stark, H., Kimmel, J. R., Krechmer, J. E., Day, D. A., Hu,
757 W., Isaacman-VanWertz, G., Yee, L., Goldstein, A. H., Khan, M. A. H., Holzinger, R., Kreisberg,
758 N., Lopez-Hilfiker, F. D., Mohr, C., Thornton, J. A., Jayne, J. T., Canagaratna, M., Worsnop, D.
759 R., and Jimenez, J. L.: Field intercomparison of the gas/particle partitioning of oxygenated
760 organics during the Southern Oxidant and Aerosol Study (SOAS) in 2013, Aerosol Sci. Technol.,
761 51, 30-56, 10.1080/02786826.2016.1254719, 2016.

762 Veres, P., Roberts, J. M., Warneke, C., Welsh-Bon, D., Zahniser, M., Herndon, S., Fall, R., and
763 de Gouw, J.: Development of negative-ion proton-transfer chemical-ionization mass
764 spectrometry (NI-PT-CIMS) for the measurement of gas-phase organic acids in the atmosphere,

765   International Journal of Mass Spectrometry, 274, 48-55, 10.1016/j.ijms.2008.04.032, 2008.

766   Voliotis, A., Wang, Y., Shao, Y., Du, M., Bannan, T. J., Percival, C. J., Pandis, S. N., Alfarra, M.
767   R., and McFiggans, G.: Exploring the composition and volatility of secondary organic aerosols
768   in mixed anthropogenic and biogenic precursor systems, Atmos. Chem. Phys., 21, 14251-14273,
769   10.5194/acp-21-14251-2021, 2021.

770   Wang, H. L., Lou, S. R., Huang, C., Qiao, L. P., Tang, X. B., Chen, C. H., Zeng, L. M., Wang,
771   Q., Zhou, M., Lu, S. H., and Yu, X. N.: Source Profiles of Volatile Organic Compounds from
772   Biomass Burning in Yangtze River Delta, China, Aerosol Air Qual. Res., 14, 818-828,
773   10.4209/aaqr.2013.05.0174, 2014.

774   Wang, M. Y., Chen, D. X., Xiao, M., Ye, Q., Stolzenburg, D., Hofbauer, V., Ye, P. L., Vogel, A.
775   L., Mauldin, R. L., Amorim, A., Baccarini, A., Baumgartner, B., Brilke, S., Dada, L., Dias, A.,
776   Duplissy, J., Finkenzeller, H., Garmash, O., He, X. C., Hoyle, C. R., Kim, C., Kvashnin, A.,
777   Lehtipalo, K., Fischer, L., Molteni, U., Petaja, T., Pospisilova, V., Quelever, L. L. J., Rissanen,
778   M., Simon, M., Tauber, C., Tome, A., Wagner, A. C., Weitz, L., Volkamer, R., Winkler, P. M.,
779   Kirkby, J., Worsnop, D. R., Kulmala, M., Baltensperger, U., Dommen, J., El Haddad, I., and
780   Donahue, N. M.: Photo-oxidation of Aromatic Hydrocarbons Produces Low-Volatility Organic
781   Compounds, Environ. Sci. Technol., 54, 7911-7921, 2020a.

782   Wang, Q. Q., He, X., Zhou, M., Huang, D. D., Qiao, L. P., Zhu, S. H., Ma, Y. G., Wang, H. L.,
783   Li, L., Huang, C., Huang, X. H. H., Xu, W., Worsnop, D., Goldstein, A. H., Guo, H., and Yu, J.
784   Z.: Hourly Measurements of Organic Molecular Markers in Urban Shanghai, China: Primary
785   Organic Aerosol Source Identification and Observation of Cooking Aerosol Aging, ACS Earth
786   Space Chem., 4, 1670-1685, 2020b.

787   Yatavelli, R. L. N., Lopez-Hilfiker, F., Wargo, J. D., Kimmel, J. R., Cubison, M. J., Bertram, T.
788   H., Jimenez, J. L., Gonin, M., Worsnop, D. R., and Thornton, J. A.: A Chemical Ionization
789   High-Resolution Time-of-Flight Mass Spectrometer Coupled to a Micro Orifice Volatilization
790   Impactor (MOVI-HRToF-CIMS) for Analysis of Gas and Particle-Phase Organic Species,
791   Aerosol Sci. Technol., 46, 1313-1327, 2012.

792   Ye, C., Yuan, B., Lin, Y., Wang, Z., Hu, W., Li, T., Chen, W., Wu, C., Wang, C., Huang, S., Qi,
793   J., Wang, B., Wang, C., Song, W., Wang, X., Zheng, E., Krechmer, J. E., Ye, P., Zhang, Z., Wang,
794   X., Worsnop, D. R., and Shao, M.: Chemical characterization of oxygenated organic
795   compounds in the gas phase and particle phase using iodide CIMS with FIGAERO in urban air,

796   Atmos. Chem. Phys., 21, 8455-8478, 10.5194/acp-21-8455-2021, 2021.

797   Zhang, X. and Seinfeld, J. H.: A functional group oxidation model (FGOM) for SOA formation
798   and aging, Atmos. Chem. Phys., 13, 5907-5926, 10.5194/acp-13-5907-2013, 2013.

799   Zhang, X., Dalleska, N. F., Huang, D. D., Bates, K. H., Sorooshian, A., Flagan, R. C., and
800   Seinfeld, J. H.: Time-resolved molecular characterization of organic aerosols by PILS plus
801   UPLC/ESI-Q-TOFMS, Atmos. Environ., 130, 180-189, 10.1016/j.atmosenv.2015.08.049,
802   2016a.

803   Zhang, X., Zhang, H. F., Xu, W., Wu, X. K., Tyndall, G. S., Orlando, J. J., Jayne, J. T., Worsnop,
804   D. R., and Canagaratna, M. R.: Molecular characterization of alkyl nitrates in atmospheric
805   aerosols by ion mobility mass spectrometry, Atmos. Meas. Tech., 12, 5535-5545, 10.5194/amt-
806   12-5535-2019, 2019.

807   Zhang, X., Krechmer, J. E., Groessl, M., Xu, W., Graf, S., Cubison, M., Jayne, J. T., Jimenez,
808   J. L., Worsnop, D. R., and Canagaratna, M. R.: A novel framework for molecular
809   characterization of atmospherically relevant organic compounds based on collision cross
810   section and mass-to-charge ratio, Atmos. Chem. Phys., 16, 12945-12959, 10.5194/acp-16-
811   12945-2016, 2016b.

812   Zhao, Y. L., Kreisberg, N. M., Worton, D. R., Isaacman, G., Weber, R. J., Liu, S., Day, D. A.,
813   Russell, L. M., Markovic, M. Z., VandenBoer, T. C., Murphy, J. G., Hering, S. V., and Goldstein,
814   A. H.: Insights into Secondary Organic Aerosol Formation Mechanisms from Measured
815   Gas/Particle Partitioning of Specific Organic Tracer Compounds, Environ. Sci. Technol., 47,
816   3781-3787, 2013.

817   Zhu, H., Wang, H., Jing, S., Wang, Y., Cheng, T., Tao, S., Lou, S., Qiao, L., Li, L., and Chen,
818   J.: Characteristics and sources of atmospheric volatile organic compounds (VOCs) along the
819   mid-lower   Yangtze   River   in   China,   Atmos.   Environ.,   190,   232-240,
820   10.1016/j.atmosenv.2018.07.026, 2018.

821   Zhu, S., Wang, Q., Qiao, L., Zhou, M., Wang, S., Lou, S., Huang, D., Wang, Q., Jing, S., Wang,
822   H., Chen, C., Huang, C., and Yu, J. Z.: Tracer-based characterization of source variations of
823   PM2.5 and organic carbon in Shanghai influenced by the COVID-19 lockdown, Faraday
824   Discuss, 226, 112-137, 10.1039/d0fd00091d, 2021.

825